Journal of Basic Physical Research ISSN: 2141-8403 Prints, 2141-8411 Online
Vol.11, No.2 pp. 1- 9, Sept., 2023. Available online at www.jbasicphyres-unizik.org

ENHANCED ELECTRICAL, MORPHOLOGY, STRUCTURAL, AND OPTICAL FEATURES OF NICKEL SILVER SULPHIDE MATERIAL FOR PHOTOVOLTAIC APPLICATIONS

Ijeh Rufus[1], Imosobomeh L. Ikhioya[2, 3*]

[1]*Department of Physics, University of Delta, Agbor, Delta State, Nigeria.*
[2]*Department of Physics and Astronomy, University of Nigeria, Nsukka, 410001, Enugu State, Nigeria.*
[3]*National Centre for Physics, Quaid-i-Azam University Campus, Islamabad, 44000, Pakistan*

Abstract
The polycrystalline NiAgS material exhibited the hexagonal wurtzite structure. The structural patterns observed at the (111), (112), (121), and (200) diffraction planes displayed diffraction peaks with angles of 26.635 º, 30.716 º, 33.875 º, and 38.018 º. The films exhibited enhanced crystallinity and increased crystallite size as the nickel molarity increased. The interaction between the transition metal and chalcogenide material leads to the creation of silver precipitate, while indications of material sublimation are evident in its original condition. The reaction between nickel and silver sulphide results in the formation of diverse-shaped condensed nanoparticles, as shown in the SEM microstructure. Higher nickel molarity leads to increased material density. Increased nickel molarity leads to higher absorbance of the synthesized material for photovoltaic use. As the nickel concentration increases, the films' absorbance also rises, enhancing the material's ability to absorb. Increased concentration of the synthesized material enhances surface area for solar and photovoltaic systems. The bandgap energy of AgS is the highest, measuring at 2.51 eV. The bandgaps of nickel at molarities of 0.1, 0.2, and 0.3 mol are 2.35 eV, 2.00 eV, and 1.66 eV, respectively.
Keywords: *Nickel; Silver, SEM; EDX; bandgap;*

Introduction

Energy is crucial for the sustainability of both the macro and micro economy. Fossil fuels make up a larger portion of energy use than renewable sources. The energy we can get from fossil fuels is limited, and there are signs indicating that they are becoming extinct due to their high depletion rate. The climate is greatly impacted by the accumulation of gases in the atmosphere caused by burning fossil fuels, which in turn affects humanity. Therefore, a complete shift from fossil fuels to renewable energy strongly promotes sustainable development goals due to the enormous negative impacts (Mayer, 2022).The utilization of renewable energy is becoming unavoidable, indicating a paradigm shift. Additionally, innovative thin-film technologies have led to cost reductions in energy conversion and storage, including solar cells, fuel cells, and lithium-ion batteries. The captivating electronic and photovoltaic applications of binary chalcogenides have generated tremendous interest in modern technology (Owusu and Asumadu-Sarkode *et al*, 2016., Holechek *et al*., 2022., Jaiswal*et al*., 2022).

The fascinating physical and electronic properties of nanostructured metal sulfides have attracted significant attention for their applications in solar cells, LEDs, batteries, sensors, and fuel cells (Younus *et al*., 2023, Hamed *et al*., 2020, Lai *et al*., 2012).Nickel sulfide, known for its stoichiometric nature, is extensively studied along with other transition metal sulfides such

*Author to whom corresponding should be addressed (I.L. Ikhioya) E-mail address: imosobomeh.ikhioya@unn.edu.ng,https://orcid.org/0000-0002-5959-4427

as CdS, Fe_2S, Co_9S_8, ZnS, and Cu_2S.NiS, also known as nickel sulphide, is a group VIII-VI compound with versatile properties as a transition metal sulfide. NiS is a crucial p-type semiconductor with a narrow optical band gap of 0.35 to 0.5 eV, making it ideal for an absorber layer (Iram *et al*., 2021, Kumar *et al*., 2018).NiS is abundant and can be dissolved in both acids and water. It is easy to process and has high electron conductivity, making it suitable for a range of technological applications because of its magnetic and electronic properties (Zhang *et al*., 2020, Krishnakumar, *et al*., 2002, Kotei, *et al*., 2022). The thin film is a 3D transition metal-insulator semiconductor that shows antiferromagnetic properties. However, it becomes paramagnetic when doped under specific temperature and pressure conditions (Gahtar *et al*., 2020).Indeed, NiS undergoes phase changes including the α-NiS and β-NiS phases, depending on temperature. These changes enable the formation of NiS_2, Ni_3S_2, Ni_3S_4, and Ni_7S_6 with varying stoichiometric ratios and oxidation states of nickel and sulfides, leading to diverse physical and chemical properties exhibited by nickel sulfides. It should be noted that the synthesis of NiS thin films becomes challenging at high temperatures because of its instability, which in turn strengthens its antiferromagnetic properties (Buchmaier *et al*., 2017., Liu, *et al*., 2014., Anuar *et al*., 2010., Krishnakum a *et al*., 2002). NiS has gained significant attention for its unique structural characteristics in energy conversion, catalysts, and as a hardening agent for semiconductor materials (Sobhani and Salavati-Niasari., 2013., Kriven, 1990). Recent research indicates that NiS is a durable and promising cathode material for lithium batteries in electric and hybrid vehicles, surpassing other options (Sartale and Lokhande., 2001). Several methods that have been adopted for the synthesis of nickel sulfide comprise thermal decomposition, successive ionic layer adsorption, and reaction, hydrothermal and solvothermal, and chemical bath deposition (Fazli *et al*., 2014., Sartale and Lokhande., 2001., Nwauzor *et al*., 2023).

Ag_2S, known as silver sulfide, is a p-type semiconductor classified as an I-VI compound. Unlike NiS, it only has a monoclinic crystal structure. Silver sulfide can be found in three different polymorphic phases: body-centered, cubic, and face-centered. Each phase exhibits different characteristics at various temperatures. The body-centered phase is stoichiometric, while the cubic and face-centered phases are non-stoichiometric. The monoclinic Ag_2S unit cell is characterized by parameters: a = 0.42264 nm, b = 0.69282 nm, c = 0.95317 nm, and β = 125.554^o. (Sadovnikov *et al*., 2015). The strong intermolecular forces within the crystal lattice make silver sulphide highly insoluble in most solvents, except for strong acids which can degrade it at room temperature. With an optical band gap between 1 and 2eV, this material possesses attractive opto-electrical properties, making it ideal for applications in photovoltaic cells, solar selective coatings, electro-luminescence, and non-linear optical devices (Ezenwa, *et al*., 2012, Moona *et al*., 2019, Yadu *et al*., 2015, Guo *et al*., 2011, Rao *et al*., 2020, Jadhav *et al*., 2013, Sahraoui *et al*., 2014).NiS and Ag_2S were synthesized together to create a suitable intermediary band gap for photovoltaic use, with longer electron diffusion lengths compared to hole lengths in the absorber layer. We chose the electrochemical method for its affordability, simplicity, quick deposition time, and improved film quality (Ijeh *et al*., 2022, Ikhioya *et al*., 2015, 2020[a], 2020[b], 2021, 2023).

Experimental Procedure

Materials and Methodology

FTO-coated glass substrates were sonicated in acetone for 25 minutes, rinsed with distilled water, and dried at 65^{o}C. Analytically graded Nickel (II) nitrate hexahydrate, ($Ni(NO_3)_2.6H_2O$), Thioacetamide (C_2H_5NS), silver nitrate ($AgNO_3$), and hydrochloric acid, magnetic stirrer, distilled water, beaker and DC power supply.

Synthesis of NiAgSmaterial

The NiAgS material was synthesized using electrochemical deposition. The working electrode, which was 2.5 cm × 1.5 cm in size and coated with FTO, was fragmented and cleaned with dishwashing liquid. Nickel (II) nitrate hexahydrate, (0.1-0.3)mol precursor, 0.99 mol solution of $AgNO_3$in 150 ml beaker, and 0.5 mol precursor of C_2H_5NS to make NiAgS. In the synthesis, a three-electrode system is used. The anode is made of platinum, the reference electrode is made of silver and silver chloride (Ag/AgCl), and the cathode is made of FTO (fluorine-doped tin oxide).The counter and reference electrodes were placed vertically in the beaker housing the FTO-coated substrate. A potentiostatic condition of -200 mV versus SCE was maintained for 15 seconds during the synthesis. A hand dryer was used to clean and dry the synthesized films. The synthesis process involved pouring target materials into beakers with equal amounts of precursors. The films were subjected to 40 minutes of annealing to eliminate internal stress. The optical characteristics, structural composition, elemental content, and electrical properties of the synthesized materials were extensively investigated with the help of suitable tools and mathematical relationships.

Results and discussion

Analysis of the hexagonal wurtzite structure of NiAgS material

The XRD pattern of the AgS and NiAgS materials is shown in Figure 1.The polycrystalline NiAgS material possessed the hexagonal wurtzite structure. The diffraction peaks at the (111), (112), (121), and (200) diffraction planes exhibited structural patterns corresponding to angles of 26.635 º, 30.716 º, 33.875 º, and 38.018 º. The crystallinity of the films was enhanced by higher nickel molarity, leading to an increase in the material's crystallite size.The structural values for the photovoltaic system's synthesized material are displayed in Table 1.The films' crystal sizes grow as the nickel molarity increases. Increasing the molarity of nickel enhances material crystallinity and promotes better photon absorption(Ijeh *et al*., 2022, Ikhioya *et al*., 2015, 2020[a], 2020[b], 2021, 2023).Equations 1-3 were used to derive the structural values in Table 1 based on the typical crystal size using Scherrer's relation.

$$D = \frac{k\lambda}{\beta Cos\theta}, \qquad 1$$

$$d = \frac{\lambda}{2sin\theta}), \qquad 2$$

$$a = d\sqrt{h^2 + k^2 + l^2}) \qquad 3$$

Figure 1(b) is depicted through XRD analysis. As the nickel molarity increases, the gradient of the Williamson-Hall graph also increases. Strain hardening causes a decrease in dislocation density, variation in crystallite size with increasing nickel concentration, and an increase in the prominent diffraction angle peak. Figure 1(c) shows the relationship between the diffraction angle and crystallite size of the material. The plot showed an inverse relationship between the material's molarity and the increase in crystal size with the diffraction angle. The larger the crystallite's size, the greater the increase in diffraction angle. The plot in Figure 1(d) displays crystal size/dislocation density against diffraction angle, revealing the precise location of the film deformation within the angle. Increasing the diffraction angle leads to bigger crystal sizes and lower dislocation density.

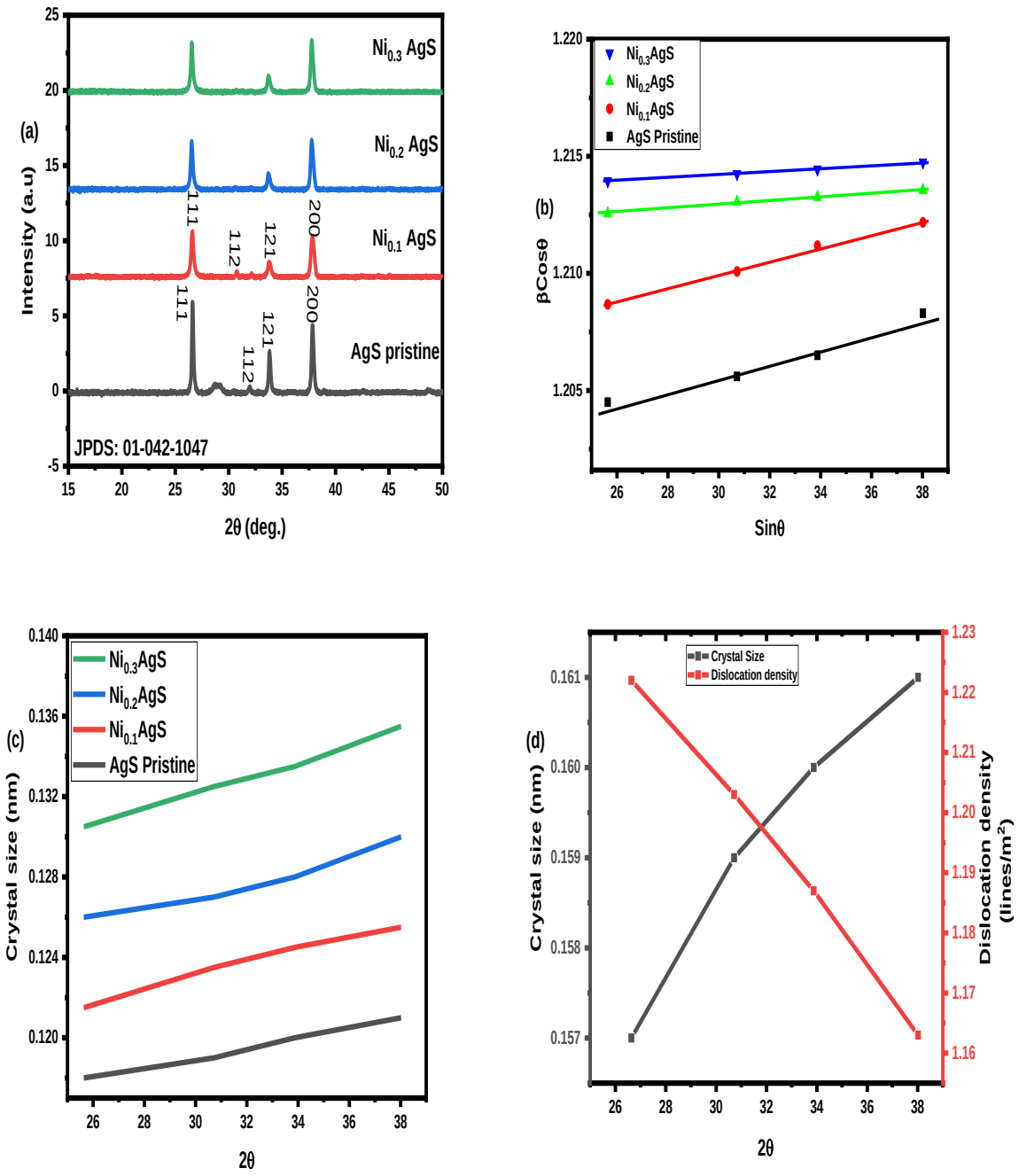

Figure 1: The XRD pattern (a), Plot of Williamson Hall (b), crystal size against 2θ (c), and (d) crystal size/dislocation density against 2θ of NiAgS material

Table 1: Structural values of NiAgS material

Films	2θ (degree)	d (spacing) Å	(Å)	(β)	(hkl)	(D) nm	**σ** lines/m^2 x 10^{16}
AgS pristine	25.431	3.501	6.065	1.2045	111	0.118	2.172
	31.992	2.797	5.594	1.2056	112	0.119	2.136
	33.745	2.655	5.311	1.2065	121	0.120	2.106
	37.811	2.378	5.319	1.2083	200	0.121	2.064
$Ni_{0.1}AgS$	26.635	3.346	5.795	0.9034	111	0.157	1.222
	30.716	2.910	5.820	0.9048	112	0.159	1.203
	33.875	2.645	5.291	0.9059	121	0.160	1.187
	38.018	2.366	5.291	0.9069	200	0.161	1.163
$Ni_{0.2}AgS$	26.635	3.346	5.795	0.9072	111	0.157	1.232
	30.716	2.910	5.820	0.9077	112	0.158	1.211
	33.875	2.645	5.291	0.9079	121	0.159	1.192
	38.018	2.366	5.291	0.9082	200	0.161	1.166
$Ni_{0.3}AgS$	26.635	3.346	5.795	0.9083	111	0.156	1.235
	30.716	2.910	5.820	0.9086	112	0.158	1.213
	33.875	2.645	5.291	0.9088	121	0.159	1.195
	38.018	2.366	5.291	0.9091	200	0.161	1.168

Surface microstructure of NiAgS material

Figure 2 (a-d) illustrates the microstructure of AgS and NiAgS. Uniform coverage on the substrate surface is achieved by depositing the material at different nickel concentrations, causing particles to clump together. The transition metal and chalcogenide material interact, resulting in the formation of silver precipitate and signs of material sublimation are visible in the pristine state of the material. Figure 2 (b) displays the SEM microstructure showing the formation of condensed nanoparticles with diverse shapes, following the reaction of nickel with silver sulphide. Increasing nickel molarity results in a higher material density. The synthesized material at $Ni_{0.1}$demonstrates how the dopant transformed the silver precipitate, showing compatibility between the two materials. However, when the dopant molarity was increased to $Ni_{0.3}$, the nanoparticle underwent restructuring, showing that surpassing $Ni_{0.3}$would reverse the material. The XRD results reveal a direct relationship between the rise in nickel molarity and the increase in crystallite size (Ijeh *et al*., 2022, Ikhioya *et al*., 2015, 2020[a], 2020[b], 2021, 2023). The results show that film syntheses have great potential for solar cell and photovoltaic applications. The material's elemental analyses are displayed in Figure 3.The spectra indicate basic elements like nickel and silver.

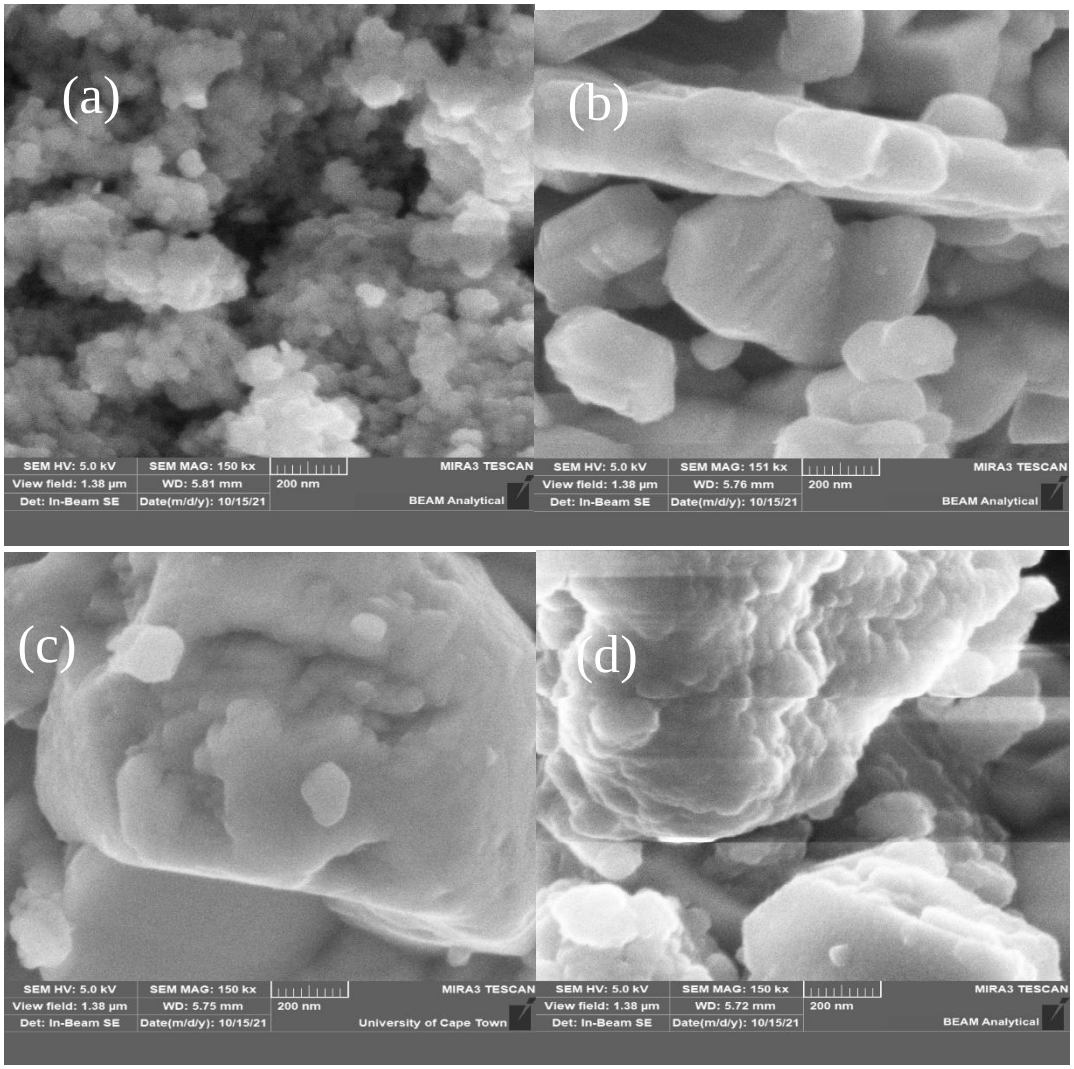

Figure 2: (a) SEM of AgS, (b) $Ni_{0.1}AgS$, (c) $Ni_{0.2}AgS$, and (d) $Ni_{0.1}AgS$

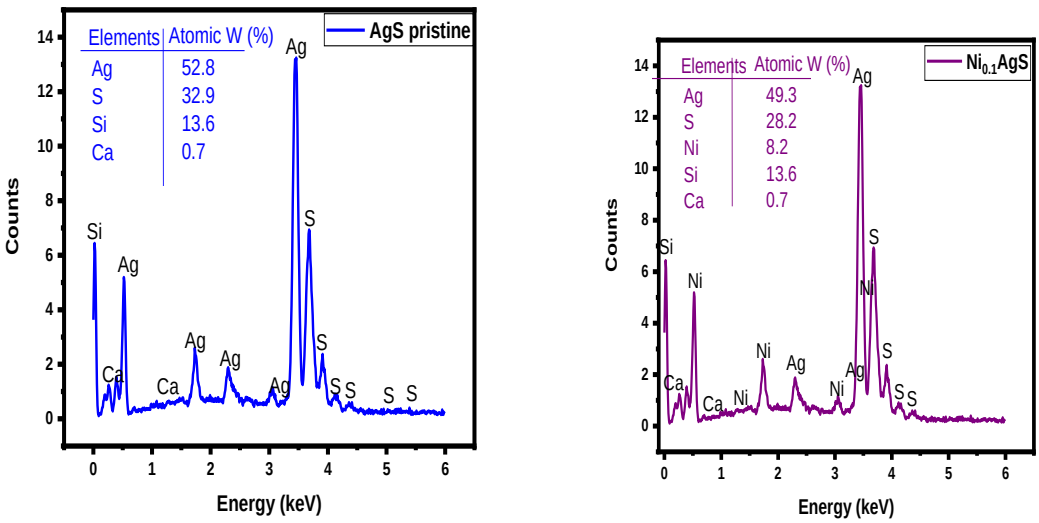

Figure 3: EDXspectra of AgS and $Ni_{0.1}AgS$

The study of NiAgS material using a photo-spectrometer.

The optical parameters were evaluated from equation (4 to 6)(Ijeh *et al*., 2022, Ikhioya *et al*., 2015, 2020[a], 2020[b], 2021, 2023).

$$A+T+R=1 \quad (4)$$

$$T = 10^{-A} \quad (5)$$

$$R = 1-(A+T) \quad (6)$$

The optical data, as observed in Figure 4, were plotted during the photo spectrometer study of NiAgS material. The absorbance spectra of NiAgS material are displayed in Figure 4(a).The impact of nickel ions on the synthesized material is highly evident. The higher the molarity of nickel, the greater the absorbance of the synthesized material for photovoltaic purposes. The films' absorbance rises as the nickel molarity increases, thus boosting the material's absorption capacity. The higher concentration of the synthesized material improves its surface area for solar and photovoltaic systems.The transmittance of the synthesized material for photovoltaics decreases as the nickel molarity increases. Increasing the nickel molarity decreases the films' transmittance and enhances the transmission of light radiation. The surface area of solar and photovoltaic systems increases due to the nickel's molarity in the synthesized material. The AgS pristine has a 75% transmittance value at 363 nm, while the material synthesized with nickel molarities of 0.1, 0.2, and 0.3mol have transmittance values of 22%, 3%, and 1.5% respectively in the UV region of the spectra. In the ultraviolet region, the spectra showed transmittance values of 98%, 66%, 42%, and 6% at a wavelength of 747 nm for AgS at concentrations of 0.1, 0.2, and 0.3 mol. The material, once fabricated, demonstrates favorable transmittance for photovoltaic systems. The reflectance of the synthesized material for photovoltaics decreases as the nickel molarity increases. Increasing the nickel molarity decreases the films' reflectance and enhances the reflection of light radiation. The surface area of solar and photovoltaic systems increases due to the nickel's molarity in the synthesized material. The AgS pristine has a 16% reflectance value at 330 nm, while the material synthesized with nickel molarities of 0.1, 0.2, and 0.3mol has negative reflectance in the UV region of the spectra. In the ultraviolet region, the spectra showed reflectance values of 5%, 20%, 5%, and -78% at a wavelength of 489 nm for AgS at concentrations of0.1, 0.2, and 0.3 mol. When a material absorbs minimal electromagnetic light radiation, it displays negative reflectance. The material is prone to transmitting light rather than reflecting it. When materials possess a high refractive index, incident light is more likely to undergo refraction instead of reflection. Negative reflectance finds applications in optical coating and solar cell advancements. Optical systems are made more efficient by minimizing surface reflection through the use of negative reflectance in optical coatings. Enhanced light absorption and increased cell efficiency result from negative reflectance in solar cells. The impact of nickel concentration on the bandgap energy of NiAgS is depicted in Figure 4(d).Among the different nickel molarities, AgS has the highest bandgap energy at 2.51 eV. The bandgaps for molarities of 0.1, 0.2, and 0.3 mol of nickel are 2.35 eV, 2.00 eV, and 1.66 eV, respectively(Ijeh *et al*., 2022, Ikhioya *et al*., 2015, 2020[a], 2020[b], 2021, 2023). The energy bandgap of NiAgS was determined using equation (7).The direct energy band gap of NiAgS was determined by projecting the line on the graph onto the photon energy axis.

$$(\propto hv)^2 = A(hv - E_g) \quad (7)$$

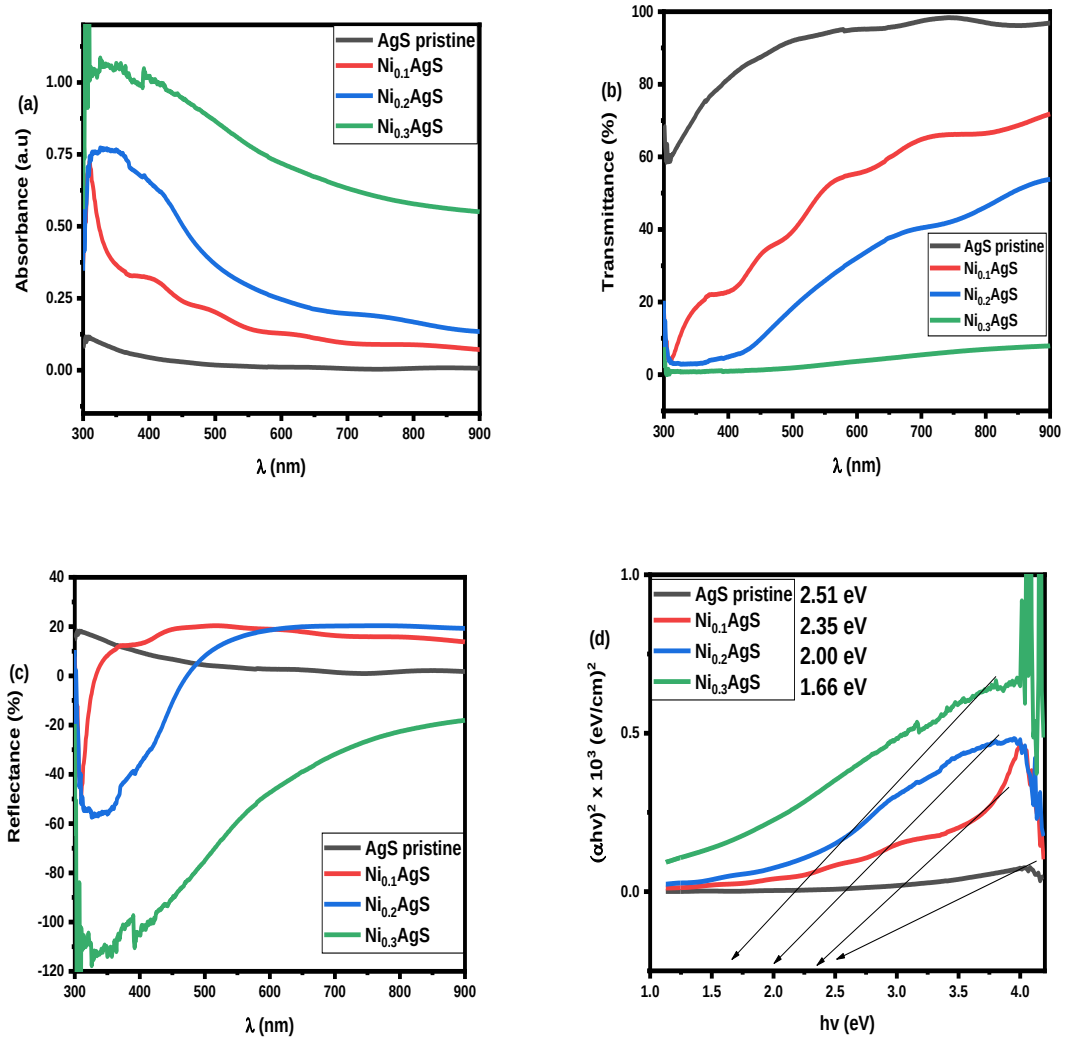

Figure 4: (a) absorbance, (b) transmittance (c) reflectance, and (d) bandgapof AgS and NiAgS

The electrical analysis of NiAgS material

The resistivity and conductivity of AgS and NiAgS material are presented in Table 2.The film's thickness rose from 106.02 to 114.26 nm, while its resistivity decreased from 16.05 to 07.78 ohm/m, resulting in a conductivity decrease from 6.23 to 1.28 S/m. The films' low resistivity and conductivity make them an excellent choice for photovoltaic and solar cell applications. Figure 5 demonstrates that as film thickness increases, there is a decrease in resistivity and conductivity. The graph demonstrates a non-ohmic relationship between resistivity, conductivity, and nickel molarity (Ijeh *et al*., 2022, Ikhioya *et al*., 2015, 2020[a], 2020[b], 2021, 2023). Figure 5 demonstrates how resistivity and conductivity change with increasing film thickness and the corresponding fluctuations in nickel molarity.

Table 2: Electrical parameters of NiAgS material

Films	**Thickness, t (nm)**	**ρ (Ω.m)x 10^7**	**σ (S/m)x 10^5**
AgS pristine	106.02	16.05	6.23
$Ni_{0.1}$AgS	109.17	11.09	9.01
$Ni_{0.2}$AgS	111.14	09.12	1.09
$Ni_{0.3}$AgS	114.26	07.78	1.28

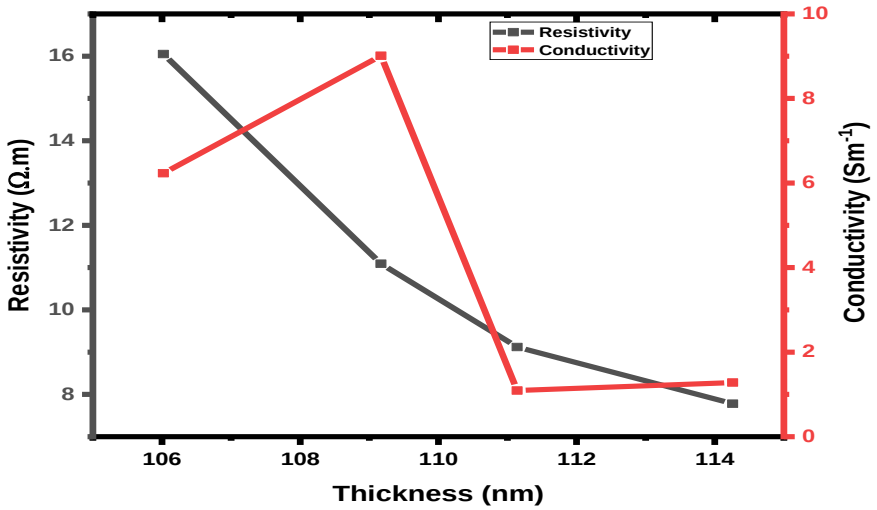

Figure 5: resistivity and conductivity against the thickness of the material

Conclusions

The successful synthesis of NiAgS material for a photovoltaic system was achieved through electrochemical deposition. In the polycrystalline NiAgS material, the structure observed was hexagonal wurtzite. The diffraction peaks at the (111), (112), (121), and (200) diffraction planes exhibited structural patterns corresponding to angles of 26.635 º, 30.716 º, 33.875 º, and 38.018 º. The crystallinity of the films was enhanced by higher nickel molarity, leading to an increase in the material's crystallite size. The transition metal and chalcogenide material interact, resulting in the formation of silver precipitate and signs of material sublimation are visible in the pristine state of the material. SEM microstructure showing the formation of condensed nanoparticles with diverse shapes, following the reaction of nickel with silver sulphide. Increasing nickel molarity results in a higher material density. The higher the molarity of nickel, the greater the absorbance of the synthesized material for photovoltaic purposes. The films' absorbance rises as the nickel molarity increases, thus boosting the material's absorption capacity. The higher concentration of the synthesized material improves its surface area for solar and photovoltaic systems. AgS has the highest bandgap energy at 2.51 eV. The bandgaps for molarities of 0.1, 0.2, and 0.3 mol of nickel are 2.35 eV, 2.00 eV, and 1.66 eV, respectively.

Acknowledgment

We are grateful to the authors for their valuable contributions to the success of the research.

References

Anuar, K., Saravanan, N., Tan, W.T., Ho, S., Teo, D. (2010). Chemical Bath Deposition of Nickel Sulphide (Ni_4S_3) Thin Films *Leonardo Journal of Sciences* 16,1-12.

Buchmaier, C., Glanzer, M., Torvisco, A., Poelt, P., Wewerka, K., Kunert, B., Gatterer, K., Trimmel G., and Rath, T. (2017). Nickel sulfide thin films and nanocrystals synthesized from nickel xanthate precursors *Journal of Material Science* 52, 10898–10914.

Chen-Ho Lai, Ming-Yen Lu and Lih-Juann Chen (2012).Metal sulfide nanostructures: synthesis,properties and applications in energy conversion and storage *Journal of Materials Chemistry*22, 19–30. DOI: 10.1039/c1jm13879k.

Ezenwa, I. A., Okereke, N. A., Egwunyenga, N. J. (2012). Optical Properties of Chemical Bath Deposited Ag_2S Thin Films *International Journal of Science and Technology* 2, 3, 101-106.

Gahtar, A., Benramache, S., Zaouche, C., Boukacham, A., Sayah, A. (2020).Effect of temperature on the properties of nickel sulfide films performed by spray pyrolysis technique *Advances in Materials Science*, 20, 3, 36-51. DOI: 10.2478/adms-2020-0015.

Guo, X., Cheng, S., Lu, P., and Zhou., H (2011). Preparation of Ag_2S thin films by electro deposition. *Material science forum*, 663, 665, 910-913

Hamed, M.S.G., Osenib, S.O., Kumar, A., Sharma, G., Mola, G.T. (2020). Nickel sulphide nano-composite assisted hole transport in thin film polymer solar cells *Solar Energy* 195 310-317.

Holechek, J. L., Geli, H.M. E., Sawalhah, M.N. and Valdez. R. (2022). A Global Assessment: Can Renewable Energy Replace Fossil Fuels by 2050? Sustainability, 14, 4792, 1-22. https://doi.org/10.1155/2022/6587934.

Ijeh, R. O., Ugwuoke, C. O., Ugwu, E. B., Aisida, S. O., Ezema, F. I. (2022). Structural, optical and magnetic properties of Cu-doped ZrO2 films synthesized by electrodeposition method *Ceramics International* 48, 4686–4692.

Ikhioya, I. L. (2015). Optical and electrical properties of ZnTe thin films using electrodeposition technique. *International Journal of Innovation Applied Studies* 12, 2, 369–373.

Iram, S., Mahmood, A., Ehsan, M., Mumtaz, A., Sohail, M., Sitara, E., Bukhari., Gul, S., Fatima, S.A., Khan, M.Z., Shaheen, R., Malik, S.N., and Malik, A. M . (2021). Impedance Spectroscopic Study of Nickel Sulfide Nanostructures Deposited by Aerosol Assisted Chemical Vapor Deposition Technique *Nanomaterials* 2021, 11, 1105. 1-14. https://doi.org/10.3390/nano11051105.

Jadhav, U. M., Patel, S. N., and Patil, R. (2013). Synthesis of Silver Sulphide Nanoparticles by Modified Chemical Route For Solar Cell Applications *Research Journal of Chemical Sciences* 3, 7, 69-74.

Jaiswal, K.K., Chowdhury, C.R., Yadav, D., Verma, R., Dutta, S., Jaiswal, K.S., Sangmesh,B., Karuppasamy, K.S K. (2022). Renewable and sustainable clean energy development and impact on social, economic, and environmental health *Energy Nexus* 7, 100118, 2-14.

Kotei, P. A., Boadi, N.O., Saah, S. A., and Mensah, M. B. (2022).Synthesis of Nickel Sulfide Thin Films and Nanocrystals from the Nickel Ethyl Xanthate Complex Advances in Materials Science and Engineering. Article ID 6587934, 1-10.

Krishnakumar, S. R., Shanthi, N., Sarma, D.D. (2002). Electronic structure of millerite NiS. Phys Rev B 66:115105. Surendran, S., Vijaya-Sankar, K. V.. John-Berchmans, L. J., and Kalai-Selvan, R. K. (2015). "Polyol synthesis of α-NiS particles and its physico-chemical properties," *Materials Science in Semiconductor Processing*, 33, 16–23.

Kriven W.M. (1990). Martensitic toughening of ceramics Materials Science and Engineering: A *2, 127, 249-255.*

Kumar, V., Sharma, D.K., Sharma, K., Dwivedi, D.K. (2018). Investigation on physical properties of polycrystalline nickel sulphide films grown by simple & economical screen-printing method *Optik* 156, 43-48.

Lai, C., Lu, M., and Chen, L. (2012). Metal sulfide nanostructures: synthesis, properties and applications in energy conversion and storage *Journal of Materials Chemistry* 22, 19-30. DOI: 10.1039/c1jm13879k

Liu, S., Shi, Q., Tong, J., Li, S ., and Li, M. (2014). Controlled synthesis of spherical α-NiS and urchin-like β-NiS microstructures *Journal of Experimental Nanoscience,* 9, 5, 447581. http://dx.doi.org/10.1080/17458080.201.49266–54475819853.

Mayer, A (2022). Fossil fuel dependence and energy insecurity *Energy, Sustainability and Society* 12, 271-13. https://doi.org/10.1186/s13705-022-00353-5.

Moona, D.G., Rehanb, S., Yeona, H.D.., Leea, S.M., Parka, S.J., Ahnb, S., Choa, Y.S. (2019). A review on binary metal sulfide heterojunction solar cells *Solar Energy Materials and Solar Cells* 200, 109963, 1-12.

Nwauzor, J. N., Nnachi, E. O., Okoroudoh, I. S., Igbo., M. E., and Babalola, A. D. (2023). Optical Characterization of Nickel Sulphide Thin Films Prepared by Chemical Bath Deposition Method *Journal of Energy Research and Reviews* 14, 1, 33-38.

Owusu, P.A., and Asumadu-Sarkode, S. (2016). A review of renewable energy sources, sustainability issues and climate change mitigation *Cogent Engineering* 3, 1-14 http://dx.doi.org/10.1080/23311916.2016.1167990.

Rao, P. S., Shivani, A., Kavitha. P(2020). Synthesis and Characterization of Nanocrystalline Nis–Sio_2 nanoparticles *Journal of Applied Chemistry* 13, 10, 49-53.

Sadovnikov, S.I., Gusev, A.I., Rempel, A.A. (2015).Artificial silver sulfide Ag_2S: Crystal structure and particle size in deposited powders *Superlattices and Microstructures* 83, 35–47.

Sartale, S.D., Lokhande., C.D. (2001). Preparation and characterization of nickel sulphide thin films using successive ionic layer adsorption and reaction (SILAR) method *Materials Chemistry and Physics* 72 101–104.

Sobhani, A., Salavati-Niasari, M (2013).. Synthesis, characterization, optical and magnetic properties of a nickel sulfide series by three different methods *Superlattices and Microstructures* 59 1–12

Sahraoui, K., Benramdane, N., Khadraoui, M., Miloua, R., Mathieu, C. (2014). Characterization of silver sulphide thin films prepared by spray pyrolysis using new precursor silver chloride. Sensors & Transducers 27, 319–325.

Yadu, G., Pathak, K. K., Deshmukh, K., and Pateria, M. A. (2015). Studies on optical and structural properties of Ag_2S films prepared by chemical bath deposition method *International Journal of Multidisciplinary Research and Modern Education* 1, 1, 296-301.

Younus,J., Shahzad,W., Ismail,B., Fazal,T., Shah,M., Iqbal, S.,Jawhari,A. H., Awwad,N. S., and Ibrahium,H. A. (2023). Engineering the optical properties of nickel sulphide thin films by zinc integration for photovoltaic applications Royal Society of Chemistry Advanced, **13**, 27415-27422.

Zhang, Q., Tian, Y., Liu, S., Yang, P., and Li, Y. (2020). First-Principles Study of the Elastic Properties of Nickel Sulfide Minerals under High Pressure *Minerals*, 10, 737, 1-12. doi:10.3390/min10090737.

Moona, D.G., Rehanb, S., Yeona, H.D.., Leea, S.M., Parka, S.J., Ahnb, S., Choa, Y.S. (2019). A review on binary metal sulfide heterojunction solar cells *Solar Energy Materials and Solar Cells* 200, 109963, 1-12.

Ikhioya, I.L., Onoh, E. U., Okoli D.N. and Ekpunobi A. J. (2023). Impact of bismuth as dopant on ZnSe material syntheses for photovoltaic application, Materials Research Innovations, https://doi.org/10.1080/14328917.2023.2180582

Ikhioya, I.L.,Nkele, A.C.,Okoro, C.F.,Obasi, C.,Whyte, G.M., Maaza, M., and Ezema, F. I. (2020). Effect of temperature on the morphological, structural and optical properties of electrodeposited Yb-doped $ZrSe_2$ thin films *Optik*, 220, , 165180, https://doi.org/10.1016/j.ijleo.2020.165180

Ikhioya, I .L., Nkele, A. C., Ezema, S. N., Maaza, M., and Ezema, F., (2020). A study on the effects of varying concentrations on the properties of ytterbium-doped cobalt selenide thin films, *Optical Materials*, vol. 101, 109731.

Ikhioya, I. L., Nkele, A. C., Chigozirim, E. M., Aisida, S. O., Maaza, M., and Ezema, F. I. (2021). Effects of Erbium on the Properties of Electrochemically-Deposited Zirconium Telluride Thin Films, 108–114, doi: 10.37256/nat.212021503.